Fabrication and electromagnetic wave absorption properties of amorphous Ni–P nanotubes*

Lu Hai-Peng(陆海鹏), Han Man-Gui(韩满贵)†, Cai Li(蔡 黎), and Deng Long-Jiang(邓龙江)

State Key Laboratory of Electronic Thin Films and Integrated Devices, University of Electronic Science and Technology of China, Chengdu 610054, *China*

(Received 3 September 2010; revised manuscript received 7 December 2010)

Amorphous Ni–P nanotubes are fabricated through electroless chemical deposition inside an anodic aluminum oxide template. The hysteresis loops of Ni–P nanotube arrays are each found to exhibit an unusual isotropic behaviour, which is believed to be due to the competition results between the shape anisotropy and the magnetostatic interaction among nanotubes. The dynamic dependence of permittivity on the frequency spectrum is fitted to the Lorentzian-type dispersion law. The permeability dispersion behaviours have been fitted based on the Kittel equation. Electromagnetic wave absorption properties of Ni–P nanotubes/paraffin composites with different values of thickness (t) are clearly shown by a three-dimensional graph. Furthermore, the bandwidths of composites with different "t" values can be well presented by a two-dimensional contour graph, which is a novel presentation form. The results show that the composites each have a good microwave absorption performance with t larger than 5.5 mm and with the frequency around 8 gigahertz.

Keywords: magnetic permeability, permittivity, microwave absorber, magnetic nanotubes

PACS: 07.55.–w, 77.22.Ch, 84.40.–x, 85.35.Kt **DOI:** 10.1088/1674-1056/20/6/060701

1. Introduction

Compared with other magnetic nanostructures (such as nanoparticles, nanowires, ultra-thin films), magnetic nanotubes have rarely been investigated. It is believed that magnetic nanotubes can find applications in nanomedicines,[1] biotechnologies,[2] ultra-high density magnetic storage devices, nanoelectromechanical systems,[3,4] etc. The syntheses of ferromagnetic nanotubes usually require porous template such as anodic aluminum oxide (AAO) templates and polycarbonate templates. Using these templates, various methods can be employed to fabricate ferromagnetic nanotubes, for instance, atomic layer deposition,[5,6] physical vapour deposition,[7] bio-nanotechnological method with the aid of magnetic bacteria,[8] etc. Among these methods, electrochemical deposition is most widely adopted.[9−11] Electroless chemical deposition is another chemical deposition technique, which is relatively rarely used.[12] In comparison with electrochemical deposition, electroless deposition possesses some advantages. For instance, neither an electrochemical station nor a conductive layer on one side of the anodic aluminum oxide (AAO) template is required before electroless deposition. Besides, it is easier to obtain tubular structure through electroless deposition, in which a pre-deposited catalytic layer on the pore wall of the AAO template is conducive to the formation of magnetic nanotubes. In contrast, the fabrication of such nanotubes through electrochemical deposition often requires the careful control over the current density.[13,14] Despite of these benefits, report about the successful fabrication of ferromagnetic nanotubes through electroless chemical deposition is still rare.[15]

In the present work, we are to demonstrate the fabrication of Ni–P nanotubes through electroless chemical deposition inside an AAO template and investigate their microwave dynamic permittivity and permeability dispersion properties. Finally, we will discuss the microwave absorption properties of Ni–P nanotubes by new presentation forms which are not found to have been employed by others.

2. Experimental details

The AAO template with a nominal pore size of 200 nm was purchased from Whatman Corp.® with

*Project supported by the National Natural Science Foundation of China (NSFC) (Grant No. 60701016), NSFC–Royal Society of UK International Jointed Program (Grant No. 60911130130), the Fundamental Research Funds for the Central Universities, China (Grant No. ZYGX2009J036), and the Prior Research of the State Key Development Program for Basic Research of China (Grant No. 2010CB334702).

†Corresponding author. E-mail: mangui@gmail.com

© 2011 Chinese Physical Society and IOP Publishing Ltd

its porosity around 30%. The thickness of AAO template is about 10 μm. The template was first immersed in a solution composed of $SnCl_2$ (10 g/L) and HCl (20 g/L) for 10 min and then rinsed with distilled water thoroughly. Next, the AAO template was further immersed in a solution containing $PdCl_2$ (1 g/L) and HCl (20 g/L) for 10 min, followed by the rinsing with distilled water. Electroless chemical deposition was carried out for 30 min to fabricate Ni–P nanotubes by keeping the AAO template in an aqueous solution of $NiSO_4.6H_2O$ (50 g/L), $NaH_2PO_2H_2O$ (20 g/L) and trisodium citrate (10 g/L) at 45 °C. The crystallization states of the Ni–P nanotubes within the AAO template were investigated using X-ray powder diffraction (XRD, Cu Kα radiation). The static magnetic properties of the nanotube array in an AAO membrane with 1 cm^2 area were characterized by a vibrating sample magnetometer (VSM). Subsequently, the AAO template was dissolved with a 5-M/L NaOH solution for 24 h and then rinsed with de-ionized water repeatedly by ultrasonic dispersion until the solution was neutralized. Consequently, Ni–P nanotube powders without the confinement of AAO template were obtained. The morphologies of the nanotubes were observed by a scanning electron microscopy (SEM) equipped with an energy dispersive X-ray spectrometer (EDS). Finally, the Ni–P nanotubes were randomly dispersed in paraffin with the nanotubes' ratio of 50 wt% in the composites. The nanotube/paraffin composite samples were pressed into a toroidal shape with an outer diameter of 7 mm and inner diameter of 3 mm for microwave measurement. The complex permittivities and permeabilities of the composite samples were measured on an Agilent Vector Network Analyser 8720 in a frequency range of 1 GHz–18 GHz.

3. Results and discussion

As shown by the SEM image in Fig. 1(a), it is clear that nanotubes have been obtained by the electroless chemical deposition method. The inner diameter of the nanotube is about 120 nm. The thickness of the nanotube is about 40 nm. The EDS spectrum in Fig. 1(b) reveals that the nanotubes are composed of Ni and P atoms. The atomic ratio of Ni to P is 76:24. The formation of Ni–P nanotubes involves the following chemical reactions:

$$SnCl_2 + PdCl_2 = SnCl_4 + Pd, \quad (1)$$

$$Ni^{2+} + 2e = Ni, \quad (2)$$

$$H_2PO_2^- + H_2O = H_2PO_3^- + 2H^+ + 2e^-, \quad (3)$$

$$H_2PO_2^- + H^+ + 2e^- = P + 2H_2O. \quad (4)$$

Once reaction (1) takes place, a thin layer of Pd atoms is deposited on the pore wall of AAO template. The Pd layer serves as a catalyst for the subsequent reactions from reaction (2) to reaction (4). As a result, Ni and P atoms are deposited onto the surface of the Pd layer, growing radially from the pore wall to the pore centre and forming nanotubes. It is necessary to note that Pd atoms are not found in the EDS measurement, which might be due to the fact that an extremely small number of Pd atoms used as catalyst have been formed on the wall of the AAO pore. However, if we look at this result from the other perspective, it can be concluded that such a tiny number of Pd atoms are enough to catalyze the formation of Ni–P nanotubes.

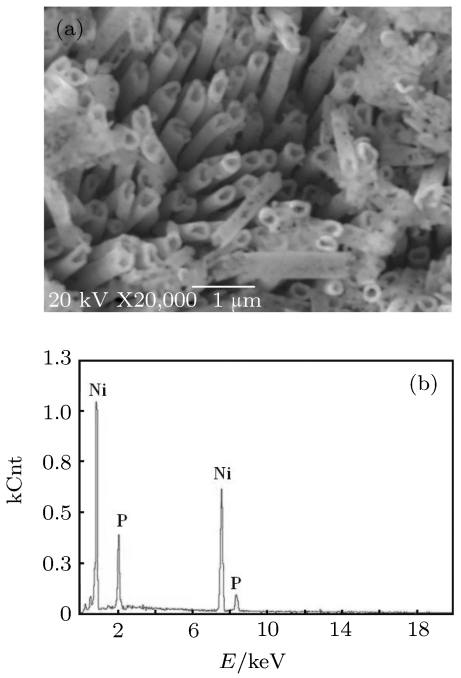


Fig. 1. (a) The SEM image of Ni–P nanotubes and (b) the EDS spectrum of the Ni–P nanotubes.

The as-prepared Ni–P nanotubes are in the amorphous state, as shown by XRD pattern in Fig. 2(a). A broad diffraction peak is at about 45° ("*A*" point), which is the fingerprint of amorphous Ni–P nanotube. The other diffraction peak at about 25° ("*B*" point) belongs to the AAO template. The XRD pattern in Fig. 2(a) indicates that the as-prepared Ni–P nanotubes are amorphous. Demonstrated in Fig. 2(b) are the hysteresis loops of the as-prepared Ni–P nanotube arrays confined in the AAO template. Two hysteresis

loops have been taken for the external magnetic field applying along two directions: H is applied along ($H_{\parallel}$) and normal to ($H_{\perp}$) the longitudinal direction. It is obvious that the static magnetic properties of amorphous Ni–P nanotubes are "nearly" isotropic from the viewpoint whether the hysteresis loops of these two measurement directions are overlapped or not. The coercivity values in the ($H_{\parallel}$) and the ($H_{\perp}$) directions are 396 Oe and 303 Oe (1 Oe=79.5775 A/m), respectively. The remanence ($M_{\rm r}/M_{\rm s}$) values of nanotubes for both measurement directions are less than 0.1. As we know, if the shape anisotropy of the nanotube dominates the magnetization reversal process, the M–H loop taken along the ($H_{\parallel}$) direction should be rectangular and the M–H loop taken along the ($H_{\perp}$) direction should exhibit almost linear behaviour and should have a very low remanence value. Such a strong anisotropy is shown by the inset in Fig. 2(b) and the differences in coercivity value and ($M_{\rm r}/M_{\rm s}$) value between the two directions are significant, which have been observed in Co nanowires:[16] the $H_{\rm c}$ values for the cases of $H_{\parallel}$ and $H_{\perp}$ are 1760 Oe and 820 Oe respectively; the ($M_{\rm r}/M_{\rm s}$) values of the cases of $H_{\parallel}$ and $H_{\perp}$ are close to 1 and 0 respectively. Compared with the values observed in Ni–P nanotube, these differences are much larger, therefore we can conclude that the prepared Ni–P nanotubes shown in this paper each exhibit an almost isotropic behaviour. As for amorphous Ni–P nanotubes, we have not observed such an anisotropic behaviour. Therefore, it can be inferred from Fig. 2(b) that the easy axis of magnetization is normal to the longitudinal direction of nanotube and there should be other factors, such as magnetostatic interaction between nanotubes, which might lead to such a nearly isotropic behaviour. Previous work revealed that magnetostatic interaction can try to align magnetic moments to be normal to the tube length direction,[9,17] competing with the shape anisotropy. Encinas-Oropesa *et al.*[17] pointed out that when the porosity of the template (p) is 1/3, the hysteresis loops will exhibit isotropic behaviour due to the strong magnetostatic interaction.[17] In our experiment, p is 30% and the distance between adjacent nanotubes is in a range of 50 nm–100 nm, accordingly it can be hypothesized that magnetostatic interaction between nanotubes in our sample plays a critical role.

The electromagnetic wave absorption properties of an absorber are strongly dependent on its high frequency complex permittivity and permeability values. The frequency (f) dependences of the relative complex permittivity for the nanotube/paraffin composite sample are given in Fig. 3(a). As shown in the figure, the permittivity dispersion is very complex. For permittivity dispersion behaviours, there are several dispersion laws depicting the dependence of ε on frequency, such as Debye law,[18] Cole–Cole law,[19] Drude law,[20] etc. It is found that the experimental results are hard to fit using one of these laws. However, we find that the Lorentzian dispersion law can give a good fitting. Since there are several permittivity dispersion peaks observed in the ε''–f spectrum, we hypothesize that there might be several dielectric relaxation processes. Each of relaxation processes might correspond to one Lorentzian-type dispersion.[21] Based on this idea, a physical model is employed for fitting, which postulates there are three Lorentzian-type dispersion processes existing in our Ni–P nanotubes/paraffin composites, the fitting can accord well with the experimental results, as shown by the dotted lines in Fig. 3(a). The fitting equation we used is given as

$$\varepsilon(f) = \sum_{i=1}^{3} \varepsilon_{\infty i} + \frac{\varepsilon_{0i} - \varepsilon_{\infty i}}{1 - {\rm i}(f/f_{{\rm d}i}) - (f/f_{{\rm r}}i)^2}, \qquad (5)$$

where ε_0 is the static permittivity, ε_∞ is the permittivity at extremely high frequency. $f_{\rm d}$ and $f_{\rm r}$ are the Debye relaxation frequency and the natural relaxation frequency respectively.

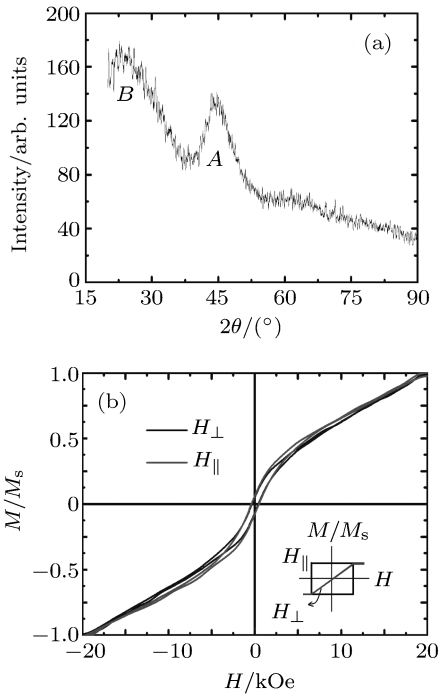


Fig. 2. The XRD pattern (a) and the VSM of the as-prepared Ni–P nanotubes within AAO templates (b).

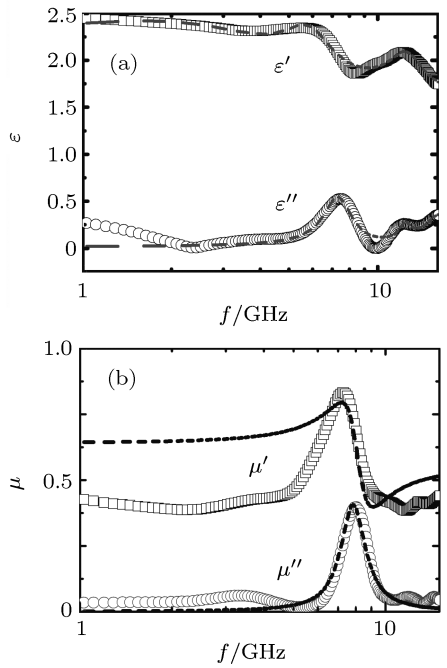


Fig. 3. (a) Permittivity spectra and (b) permeability spectra, where open symbols denote experimental results and lines represent fitting results.

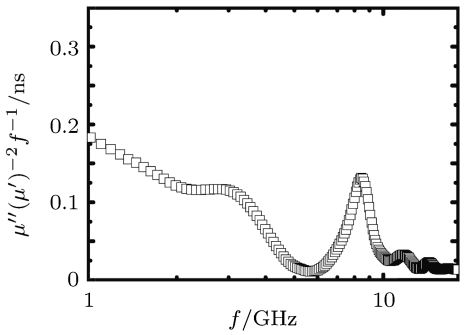


Fig. 4. The value of $\mu''(\mu')^{-2}f^{-1}$ as a function of frequency.

The permeability spectra of the nanotube/paraffin composite samples are shown in Fig. 3(b). The imaginary part (μ'') shows a major peak around $f = 7.94$ GHz and some minor fluctuations elsewhere. The real part (μ') exhibits an obvious peak at 7.15 GHz. In the GHz region, the magnetic loss can be caused by the natural resonance and eddy current effect. To determine whether the eddy current effect is a contributor, we need to evaluate the value of $C = \mu''(\mu')^{-2}f^{-1}$. If "$C$" remains constant when the frequency is varied, then the eddy current effect will lead to magnetic loss.[22] Figure 4 depicts the value of C for the sample, which varies drastically in the whole frequency range, meaning that the eddy current effect is suppressed in the measured frequency range. So the resonance peaks in Fig. 3(b) can be ascribed to the natural resonance mechanism or other mechanisms, rather than the eddy current effect.

The high frequency permeability of a ferromagnetic material depends on many factors, such as the saturation magnetization, magnetic moment configuration, magnetic anisotropy, damping constant, induced eddy current, etc. In order to interpret the experimental results, we have fitted the permeability spectra using the Kittel equation as[23]

$$\mu(f) = 1 + \frac{\chi_0(1 + \mathrm{i}\,\alpha f/f_\mathrm{r})}{(1 + \mathrm{i}\,\alpha f/f_\mathrm{r})^2 - (f/f_\mathrm{r})^2}, \qquad (6)$$

where f is the frequency, f_r is the well-known natural resonance frequency, α is the damping constant and χ_0 is the static magnetic susceptibility. The fitting results from the μ''–f spectrum for χ_0, α, and f_r are 0.09, 0.113, and 7.89 GHz respectively. All these values are in a reasonable range. The measured f_r value is 7.94 GHz, while the value of f_r obtained from fitting is 7.89 GHz. With the fitted parameters, the μ'–f spectrum is then calculated. The fitted curves, to some extent, accord well with the experimental results. Besides, our fitted natural resonance frequency (7.89 GHz) is close to that found in $Ni_{90}Fe_{10}$ nanowires (8.2 GHz–11.7 GHz) by Xiao *et al.*[24] To justify the natural resonance frequency (f_r) further, the f_r value of Ni–P nanotube can be roughly calculated based on the simplified equation: $f_\mathrm{r} = \gamma\sqrt{(4\pi M_\mathrm{s} + H_\mathrm{k})H_\mathrm{k}}$, where γ is the gyromagnetic ratio (8.79×10^6 Oe·s) and H_k is the magnetocrystalline anisotropy field. Since we do not have H_k and M_s values of Ni–P nanotube, we use the values of Ni for the rough calculation: M_s is 4.78×10^2 Gs (1 Gs=10^{-4} T) and H_k is 2×10^2 Oe. The natural resonance frequency is roughly calculated to be about 9.79 GHz, which is close to the one fitted (7.89 GHz) in Fig. 3(b). The difference in f_r value between the calculation and the fittings might originate from the rough values of H_k and M_s. Moreover, there are minor fluctuations observed in the experimental permeability spectra deviating from the fitted curve, which might be associated with the different magnetic moment configurations in the special hollow structure of nanotubes. Similarly, other investigators have pointed out based on the micromagnetism simulations of magnetic nanostructures (such as nanowires, nanorings) that the inhomogenous magnetic moment configurations along a nanostructure element could result in different peaks in a magnetic permeability dispersion spectrum, such as the central part and the two ends

of a nanowire can result in different dispersion peaks at different frequencies in the μ–f spectrum but the frequencies of dispersion peaks due to this mechanism are usually larger than 20 GHz.[25−27] Therefore we can conclude that the observed peak in the μ–f is due to the natural resonance peak.

The electromagnetic wave absorption property of an absorber is dependent on six parameters, such as the thickness (t) of the absorber, ε', ε'', μ', μ'', and frequency (f). The criterion of absorption performance usually is expressed by the reflection loss ($\Gamma_{\rm RL}$) in dB unit. Based on the measured complex permittivity and permeability and on the assumption that a single layer of Ni–P nanotubes/paraffin composite is attached to a metal plate, the electromagnetic wave absorption properties can usually be evaluated by the following equation:[28,29]

$$\Gamma_{\rm RL} = 20\log|(Z_{\rm in} - Z_0)/(Z_{\rm in} + Z_0)|\,, \qquad (7)$$

where Z_0 is the impedance of free space and $Z_{\rm in}$ is the input impedance of the absorber, which can be expressed as

$$Z_{\rm in} = Z_0\sqrt{\mu_{\rm r}/\varepsilon_{\rm r}}\tanh\{j(2\pi ft/c)\sqrt{\mu_{\rm r}\varepsilon_{\rm r}}\} \qquad (8)$$

with c being the speed of light. Figure 5(a) is a three-dimensional graph which clearly shows the electromagnetic wave absorption properties of Ni–P nanotube/paraffin composite with different thicknesses within the measurement frequency range of 1 GHz–18 GHz. The grey colour bar in Fig. 5(a) indicates different $\Gamma_{\rm RL}$ values in dB unit corresponding to different colours. For many applications, the $\Gamma_{\rm RL}$ value smaller than −10 dB is acceptable. Figure 5(b) clearly shows the bandwidths ($\Gamma_{\rm RL} < -10$ dB) of electromagnetic wave absorption for absorbers with different thicknesses. For instance, when t is 5 mm, the bandwidth with the $\Gamma_{\rm RL}$ value less than −10 dB is 0. When t is 7 mm, the bandwidth is in a range of 7.15 GHz–8.90 GHz, as shown the "a–b" section in Fig. 5(b). By this method, it is very handy to obtain an overall knowledge on the bandwidth of any absorber with any thickness. It should be noted that figure 5(b) has a different grey colour bar. This is because in order to show the bandwidth with $\Gamma_{\rm RL}$ less than −10 dB, its colour bar in Fig. 5(b) must start with a colour on the right end side corresponding to −10 dB.

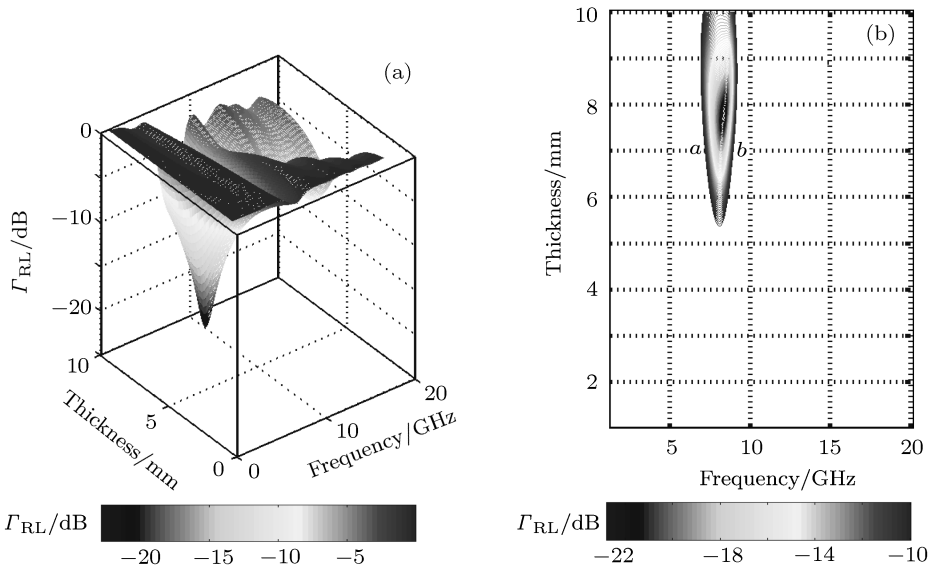


Fig. 5. Microwave absorption properties of Ni–P nanotubes: (a) three-dimensional illustration; (b) the bandwidth with the $\Gamma_{\rm RL}$ value smaller than -10 dB.

4. Conclusions

Amorphous Ni–P nanotubes have been successfully fabricated by an electroless chemical deposition method. The measured magnetic hysteresis loops show that the Ni–P nanotube array exhibits an isotropic behaviour. The complex relative permittivity and permeability dispersion behaviours have been studied within 1 GHz–18 GHz. The dependence of permittivity on frequency can be explained by the multi Lorentzian dispersion law. The permeability dispersion spectra can be fitted to the Kittel equation. The effect of eddy current on high frequency permeability is found not to play a role. Finally, we

have presented that it is easier to find the bandwidths of absorbers with different thicknesses by using a two-dimensional graph, which can be useful for designing electromagnetic wave absorbers.

References

[1] Gasparac R, Kohli P, Mota M O, Trofin L and Martin C R 2004 *Nano Lett.* **4** 513

[2] Haberzettl C A 2002 *Nanotechnology* **13** R9

[3] Khizroev S, Kryder M H, Litvinov D and Thompson D A 2002 *Appl. Phys. Lett.* **81** 2256

[4] Sui Y C, Skomski R, Sorge K D and Sellmyer D J 2004 *J. Appl. Phys.* **95** 7151

[5] Escrig J, Daub M, Landeros P, Nielsch K and Altbir D 2007 *Nanotechnology* **18** 445706

[6] Escrig J, Bachmann J, Jing J, Daub M, Altbir D and Nielsch K 2008 *Phys. Rev.* B **77** 214421

[7] Wang S, Yu G J, Gong J L, Li Q T, Xu H J, Zhu D Z and Zhu Z Y 2006 *Nanotechnology* **17** 1594

[8] Banerjee I A, Yu L, Shima M, Yoshino T, Takeyama H, Matsunaga T and Matsui H 2005 *Adv. Mater.* **17** 1128

[9] Tao F, Guan M, Jiang Y, Zhu J, Xu Z and Xue Z 2006 *Adv. Mater.* **18** 2161

[10] Bao J, Tie C, Xu Z, Zhou Q, Shen D and Ma Q 2001 *Adv. Mater.* **13** 1631

[11] Wang X W, Yuan Z H, Sun S Q, Duan Y Q and Bie L J 2008 *Mater. Chem. Phys.* **112** 329

[12] Ren X, Jiang C H, Huang X M and Li D D 2009 *Physica* E **41** 349

[13] Li D D, Thompson R S, Bergmann G and Lu J G 2008 *Adv. Mater.* **20** 4575

[14] Bao J, Tie C, Xu Z, Zhou Q, Shen D and Ma Q 2001 *Adv. Mater.* **13** 1631

[15] Ren X, Jiang C H, Huang X M and Li D D 2009 *Physica* E **41** 349

[16] Zhang J, Jones G A, Shen T H, Donnelly S E and Li G 2007 *J. Appl. Phys.* **101** 054310

[17] Encinas-Oropesa A, Demand M, Piraux L, Huynen I and Ebels U 2001 *Phys. Rev.* B **63** 104415

[18] Jonscher A K 2008 *Dielectric Relaxation in Solids* (Xi'an: Xi'an Jiaotong University Press) p. 96

[19] Cole K S and Cole R H 1941 *J. Chem. Phys.* **9** 341

[20] Dragoman D and Dragoman M 2006 *J. Appl. Phys.* **99** 076106

[21] Han M G, Ou Y, Liang D F and Deng L J 2009 *Chin. Phys.* B **18** 1261

[22] Wu M Z, Zhang Y D, Hui S, Xiao T D, Ge S H, Hines W A, Budnick J I and Tayor G W 2002 *Appl. Phys. Lett.* **80** 4404

[23] Li Z W, Lin G Q, Chen L F, Wu Y P and Ong C K 2005 *J. Appl. Phys.* **98** 094310

[24] Kou X, Fan X, Zhu H and Xiao J Q 2009 *Appl. Phys. Lett.* **94** 112509

[25] Liu R, Wang J, Liu Q, Wang H and Jiang C 2008 *J. Appl. Phys.* **103** 013910

[26] Gérardin O, Le Gall H, Donahue M J and Vukadinovic N 2001 *J. Appl. Phys.* **89** 7012

[27] Chen W B, Han M G, Zhou H, Ou Y and Deng L J 2010 *Chin. Phys.* B **19** 087502.

[28] Naito Y and Suetake K, 1971 *IEEE Trans. Microwave Theory Technol.* **19** 65

[29] Tsay C Y, Yang R B, Hung D S, Hung Y H, Yao Y D and Lin C K 2010 *J. Appl. Phys.* **107** 09A502